Available online at www.sciencedirect.com
SCIENCE DIRECT®
Ocean Modelling 11 (2006) 28–48
Ocean Modelling
www.elsevier.com/locate/ocemod

Enhancing the resolution of sea ice in a global ocean GCM

Achim Stössel *, Joong-Tae Kim

Department of Oceanography, Texas A&M University, 3146 TAMU, College Station, TX 77843, USA

Received 20 October 2004; received in revised form 21 October 2004; accepted 16 November 2004
Available online 18 December 2004

Abstract

Open water in sea ice, such as leads and polynyas, has a considerable impact on the long-term global deep-ocean properties and circulation. Its representation in ocean general circulation models (GCMs) that are designed for studies of the long-term thermohaline circulation, however, bears large uncertainties. Here, an attempt has been made to reduce such uncertainties by enhancing the resolution of the sea-ice component, while keeping the ocean component at coarse resolution to preserve the necessary efficiency of the GCM. In this study, the higher-resolved sea-ice component has been restricted to the Southern Ocean. Compared to the original model, the new version yields more detailed structures, such as a more detailed representation of coastal polynyas, a realistically sharp ice edge, and an overall enhanced lead fraction. The latter gives rise to a somewhat enhanced rate of Antarctic Bottom Water formation through enhanced near-boundary convection, which is reflected in slightly cooler and fresher global deep-ocean properties and a reduced Antarctic Circumpolar Current as a result of reduced open-ocean convection. Sensitivity studies reveal that it is not the overall enhanced lead fraction but rather the coastal katabatic winds that lead to this behaviour of the higher-resolution model. Artifacts resulting from the coarse-grid coastline were minimized in a separate model version where fine surface grid cells of fast ice were introduced following the fine-grid land/ice-shelf—sea-ice/ocean boundary of satellite-derived microwave data. This study represents an intermediate step toward resolving the sea-ice component of a global coarse-resolution ocean GCM on a scale of about 30 km.
© 2004 Elsevier Ltd. All rights reserved.

* Corresponding author. Tel.: +1 979 8624170; fax: +1 979 8478879.
E-mail address: astoessel@ocean.tamu.edu (A. Stössel).

1463-5003/$ - see front matter © 2004 Elsevier Ltd. All rights reserved.
doi:10.1016/j.ocemod.2004.11.004

1. Introduction

High-latitude surface conditions play a crucial role in determining the long-term deep-ocean properties and circulation of the world's ocean (e.g., Maier-Reimer, 1993; Broecker, 1997; Duffy et al., 1999; Goosse et al., 2001; Orsi et al., 2001; Stössel et al., 2002). Such conditions are to a large extent controlled by the presence of sea ice, in particular by processes associated with its formation and melting, and its drift and dynamic compression. Of particular importance is the occurrence of leads and polynyas (e.g., Comiso and Gordon, 1998; Markus et al., 1998; Eisen and Kottmeier, 2000; Goosse and Fichefet, 2001; Renfrew et al., 2002). These can be a product of divergent ice drift, either near the shore line or in the open ocean, or of oceanic heat flux, e.g. in conjunction with convective plumes.

Ocean general circulation models (GCMs) typically used for climate studies and studies of the global thermohaline circulation are unable to resolve leads and polynyas. Rather, such are parameterized as open-water fraction per grid cell of a sea-ice model that is coupled to the ocean GCM (e.g., Marsland et al., 2003). Higher resolution (sea-ice)—ocean GCMs would be a logic step toward a more detailed representation of open water in the ice pack. This, however, is not feasible because of the long deep-ocean adjustment time which constrains an ocean GCM designed for thermohaline circulation studies to coarse resolution. Here we present a compromise in which the resolution of merely the sea-ice component is enhanced, thereby refining the representation of leads and polynyas, while retaining the ocean model efficient enough to conduct investigations on the impact of high-latitude processes on global deep-ocean properties and circulation.

An alternative approach would be to nest a high-resolution high-latitude model into a coarse-resolution global ocean GCM. Several regional Southern Ocean models would indeed be available for such purpose (e.g., Beckmann et al., 1999; Marsland and Wolff, 2001; Timmermann et al., 2002). While appealing at first glance, literature on nested models indicates still substantial technical problems, in particular when it comes to two-way nesting (e.g., Spall and Holland, 1991; Fox and Maskell, 1996; Jacob and Podzun, 1997; Feser et al., 2001), which would need to work properly in long-term model integrations on the order of 1000 years.

A numerically more consistent alternative is the usage of a global curvilinear grid with stereographic projection and the poles located over land close to regions that are to feature higher resolution (Maier-Reimer, 1997; Mikolajewicz et al., 2001; Marsland et al., 2003). Unfortunately, this approach suffers from the serious time-step limitation required for numerical stability, and is thus not suitable for long-term studies on changes of global deep-ocean properties.

The particular focus of this study is on a higher-resolution model representation of Southern Ocean sea ice. The main motivation here is to arrive at a more accurate estimate of the surface buoyancy fluxes that ultimately drive convection and bottom-water formation, recalling that these fluxes are highly dependent on the sea-ice concentration, and the ice-thickness distribution. Investigating through which mechanism the higher-resolution sea ice modifies global deep-ocean properties, the decisive factor turns out to be how Antarctic Bottom Water (AABW) is predominantly formed in the model, i.e., whether it is mostly formed by open-ocean convection as opposed to near-boundary convection (Carmack, 1990). The latter process, involving brine release due to freezing, mainly in coastal polynyas, and the accumulation of (high salinity) shelf water, is considered to play the dominant role in the formation of AABW under present-day climate conditions (e.g., Gordon, 1998).

This study constitutes an intermediate step toward a resolution of 30 km, which is close to the pixel resolution of satellite passive microwave data from which ice concentration is routinely derived (Gloersen et al., 1992; Comiso, 1995; Markus and Cavalieri, 2000). The final step is to allow for a rigorous evaluation of the simulation of sea ice in a global ocean GCM, sea ice acting as a sensitive gauge for the quality of the global simulation. This study is to demonstrate that global simulations with a 'nested' higher-resolution sea-ice component are robust and promising enough to envision the next step of resolution enhancement. Given the fact that leads and polynyas occur on relative small scales, that they are highly variable in time and space, and that they constitute the locations of most vigorous heat loss in fall and winter, a higher-resolution sea-ice component is also worthwhile to be aimed at in view of a coupling with the atmosphere. The approach presented here might thus also become useful for the next generation of coupled climate GCMs.

The model and its refinement is described in the next section. The results in Section 3 are to illustrate the impact of a successively finer representation of sea ice around Antarctica, i.e. its spatial resolution followed by a refinement of the coastline. Section 4 deals with sensitivity studies that aim at identifying the reasons for the differences in the global response with a change in the grid resolution of Southern Ocean sea ice. Conclusions and an outlook are provided toward the end.

2. The model

A global coarse-resolution version of the Hamburg Ocean Primitive Equation (HOPE) model is the starting point for the new model setup. This version is identical to that described in Stössel et al. (2002), which is a majorly revised offspring of the version of Drijfhout et al. (1996). An overall revised and curvi-linear version of this model is described in Marsland et al. (2003). The sea-ice component includes thermodynamics following Owens and Lemke (1990) and viscous-plastic dynamics based on Hibler (1979). Crucial for the coupling of the atmospheric fields to the ocean is the detailed surface heat balance calculation, which features a subgrid distinction between the open-water and ice-covered part of a model grid cell. The overall heat flux per grid cell is thus a direct function of the modelled ice concentration. In order to capture leads created by atmospheric synoptic processes, the wind forcing over the Southern Ocean is provided by daily analyses fields of the European Centre for Medium Range Weather Forecasts (ECMWF) of one year. Otherwise, the momentum, heat and fresh-water flux are based on monthly climatological fields (see Stössel et al., 2002). Furthermore, the model includes a subgrid-scale plume convection parameterization following Paluszkiewicz and Romea (1997) (Kim and Stössel, 2001).

As a first attempt of a higher-resolution sea-ice model "nested" in a coarse-resolution ocean model, we enhanced the resolution of the sea-ice model by a factor of 9, i.e. each (upper-layer) ocean grid point is coupled to 9 sea-ice grid points. The way this is realized on the Arakawa E-grid of the model is illustrated in Fig. 1. This procedure reduces the grid spacing from approximately 200 km to 80 km. For the reason given in Section 1, we introduced this only in the southern hemisphere south of 50 S, north of which sea ice does normally not occur (Gloersen et al., 1992). In order to avoid artificial gradients across coarse grid-cell borders, all atmospheric forcing fields are smoothed over 9 fine grid points, respectively. All relevant oceanic fields are converted from the coarse to the fine grid each time step before sea ice is integrated forward. This procedure

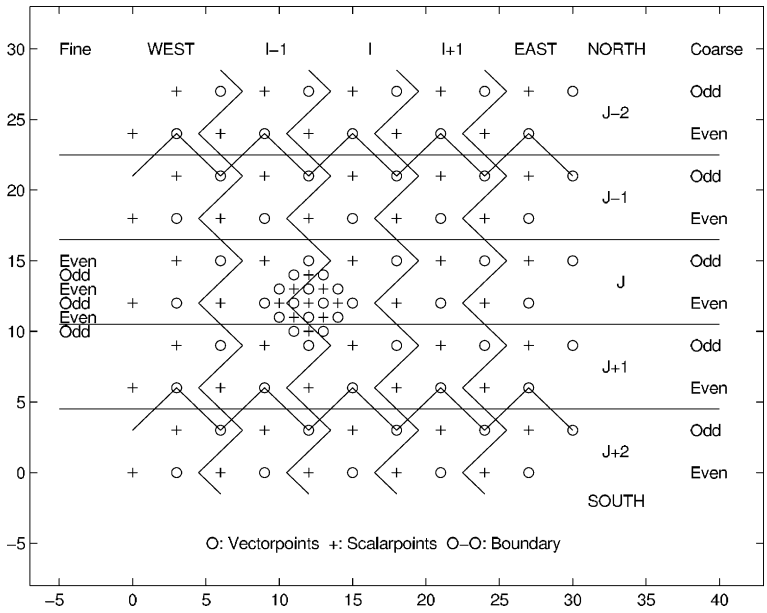

Fig. 1. 9-fold resolution enhancement in Arakawa E-grid. The embedded finer resolution of the sea-ice component is shown for the coarse even scalar point I, J. The underlying graph is from Wolff et al. (1997).

involves smoothing of the ocean currents and the sea-surface height (which is a prognostic quantity in the 'free-surface' ocean GCM used here). Each time step the prognostic sea-ice calculation is completed, its impact on the ocean requires a conversion of the affected ocean variables to the coarse grid, which involves a simple averaging procedure. Note that in order to preserve their fine-grid properties during the prognostic time-stepping, the sea-ice variables are not subject to this conversion procedure.

While the conversion described above enhances the resolution of the OGCM's sea-ice component, the ocean is still calculated on the coarse grid, which implies that the coastline (around Antarctica) is limited in its resolution by the coarse grid. This leads to artifacts along the coastline that may reduce the benefits of simulating sea ice with higher resolution along the coast. In particular, the locations of the coastal polynyas may not be represented all that much more realistic with the higher resolution model than with the coarser resolution one. To improve this situation, an additional model version has been created in which the coastal ocean grid columns are partially being covered at their surface following the finer ice shelf/land margin of satellite-derived passive microwave data (in particular the Special Sensor Microwave Imager, SSM/I; e.g., Markus and Cavalieri, 2000). This cover is specified to essentially inhibit any momentum, heat, and fresh-water flux between atmosphere and ocean by specifying it as fast ice with a thickness of 1 meter. This procedure required a prior "excavation" of coarse-grid coastal grid points where the SSM/I data shows sea ice or open water and the coarse model land. Conversely, ocean grid points were filled where they are entirely within the SSM/I boundary. This resulted in net 15 additional ocean columns (wet points). Since the center of the new wet grid points is geographically located over land, these points had to be provided with a water depth, which was chosen to be 450 m. Their volume has been adjusted to fit the actual bathymetry more realistically by reducing the depth of the water

column linearly by the number of fine grid cells being covered by fast ice. That is, if 8 of the 9 fine surface cells are fast ice, the depth of such water column is reduced to 50 m. This measure is to (crudely) compensate for the fact that the volume of a (coarse) coastal ocean grid point cannot be adjusted to a finer coastline by filling it up laterally. [1] Because of the change in the number of wet points, the results of the new equilibrium integration feature changes in the ocean's circulation and properties that are not solely due to the finer sea-ice coastline.

3. Results

First, we will compare results from the coarse ocean—coarse sea ice—coarse coastline (CCC) model with those from the coarse ocean—fine sea ice—coarse coastline (CFC) model. In the second subsection, we will turn to the coarse ocean—fine sea ice—fine coastline (CFF) model. All model results shown represent cyclostationary equilibrium solutions attained after global model integrations on the order of 1000 years.

3.1. CCC versus CFC

For a direct comparison of the CFC results with those of CCC, the CFC results are converted to coarse grid following the procedure described in Section 2. For ice concentration during the time of maximum ice extent in September (Fig. 2a, b versus 3a, b) one finds that there are no fundamental differences. Compared to corresponding satellite-derived products (Fig. 6), CFC does better in the Indian Ocean sector. The ice extent of the Weddell Sea is underestimated in both cases.

The open-water areas (polynyas) within the ice pack emerging in the daily snapshots are due to plume convection, which emerges sporadically, and lasts for a few days until the phase of "lateral exchange" (Marshall and Schott, 1999) sets in and the water column gradually retains stable stratification. That plumes, or rather the resulting "mixed patches" or "chimneys" (Marshall and Schott, 1999, and literature referenced therein) should have such a large effect on the sea-ice cover has not been manifested from observations. The potential validity of this feature has been discussed in Stössel and Markus (2004). This feature does also occur with the 9-fold higher sea-ice resolution, though somewhat less pronounced (see Section 4).

The actual benefit of using CFC rather than CCC becomes obvious when illustrating the CFC results at the actual fine-grid resolution (Fig. 4a, b). Now details become apparent that cannot be resolved with CCC. Most striking are a larger abundance of coastal polynyas, and a sharp ice edge, both of which resemble more closely the satellite-derived product (Fig. 6). The ice-thickness distribution as well features much more detail (Figs. 2–4c), mainly because the nonlinear ridging processes that occur under dynamic compression are now simulated on a finer grid. One can also extract that ridging against coastline extensions that are part of a bay occurs simultaneously with polynya formation at the opposite side of the bay. These features compare well with observations,

[1] It should be noted in this context that the HOPE model features "partial grid cells" (a la Griffies et al., 2000), i.e. each water column has its own depth following the actual bathymetry rather than the vertical resolution of the model (Maier-Reimer et al., 1993).

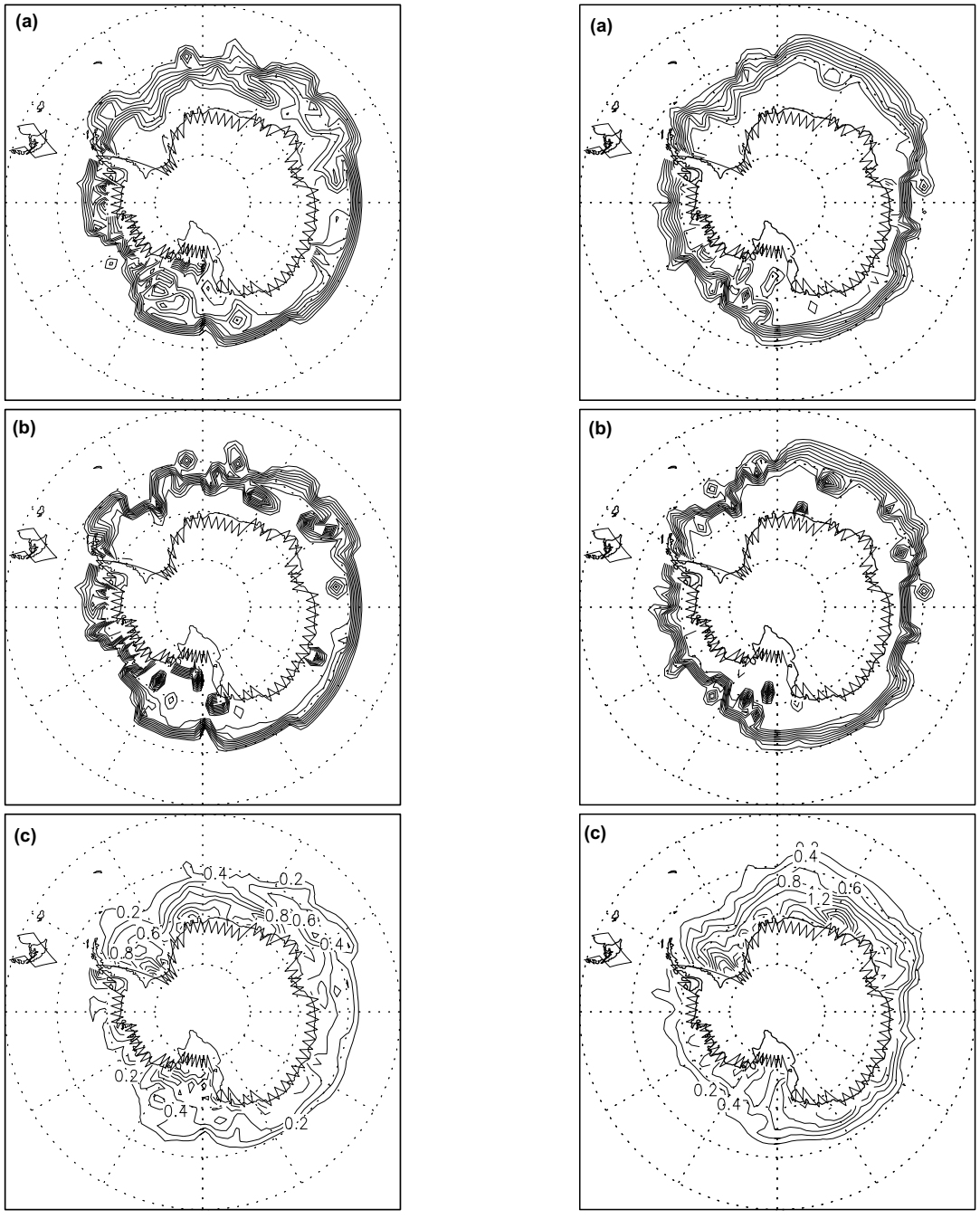

Fig. 2. September mean (a) and mid-September (b) ice concentration, as well as September mean ice thickness (c) as simulated with CCC (see text). The isolines of ice concentration range from 10% to 100% with an increment of 10%.
Fig. 3. Same as Fig. 2, but as simulated with CFC, displayed on coarse grid.

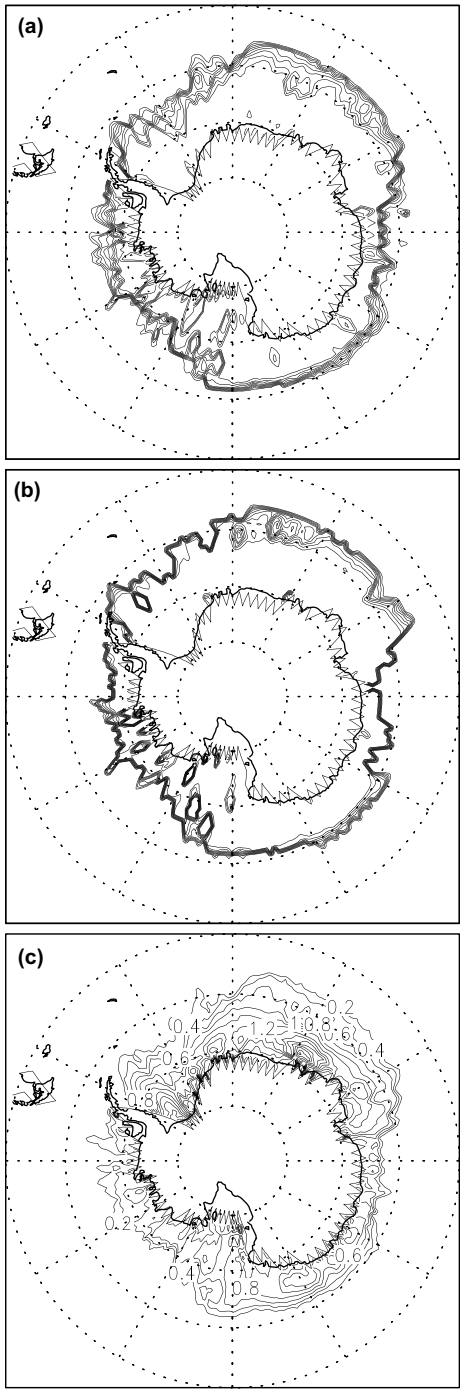

4

Fig. 4. Same as Fig. 3, but displayed on fine grid.

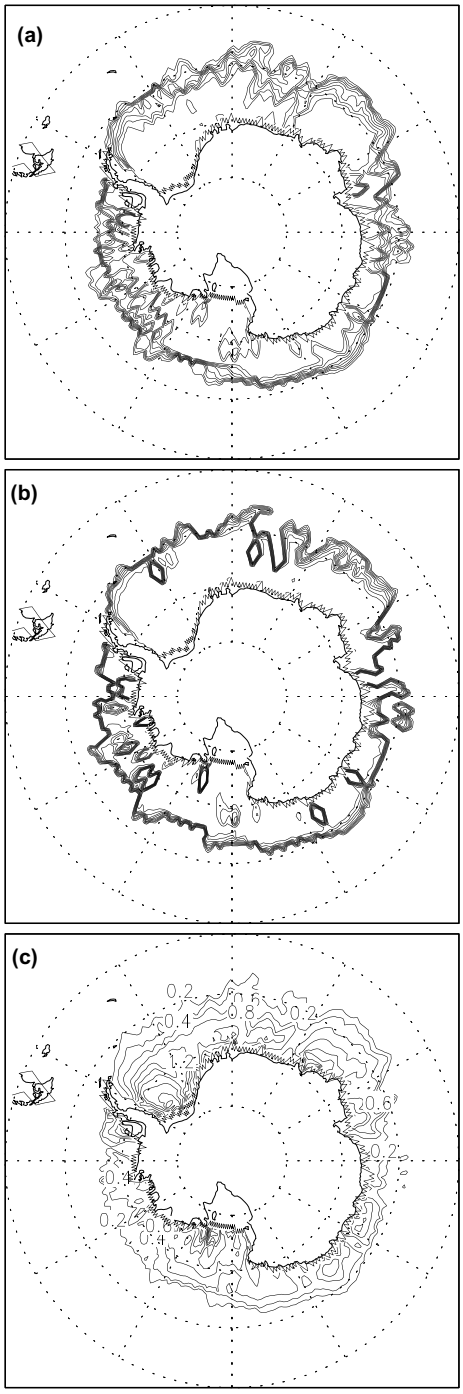

5

Fig. 5. Same as Fig. 4, but as simulated with CFF.

Table 1
Selected annual mean choke point numbers of the thermohaline circulation for the listed experiments (abbreviations explained in text)

Exp.	NADW outflow [Sv]	DP throughflow [Sv]	$\Theta_{4000\ m}$ [degC]	$S_{4000\ m}$ [psu]
CCC	12.1	105	1.43	34.746
CCC/V	11.1	108	1.26	34.750
CCC/L	10.7	112	1.11	34.749
CCC/CP	11.3	110	1.26	34.747
CCC/K	11.1	107	1.15	34.730
CFC	11.5	97	1.30	34.720
CFC/V	11.1	99	1.25	34.732
CFF	10.5	81	0.56	34.657

NADW outflow is the southward flow of NADW across 30 °S in the Atlantic. DP stands for Drake Passage (the throughflow through which is a measure for the strength of the ACC). $\Theta_{4000\ m}$ and $S_{4000\ m}$ represent the global mean potential temperature and salinity at 4000 m depth, respectively.

as e.g. in the Bay and Sea of Bothnia, where winter navigation is always directed along the coastline of polynya occurrence (e.g., Kalliosaari and Seinä, 1987).

In terms of any long-term, global impacts of refining the sea-ice grid in the Southern Ocean, some choke point numbers are provided in Table 1 (CCC versus CFC). There is a slight reduction (0.6 Sv) of the North Atlantic Deep Water (NADW) outflow going along with a reduction of the Drake Passage throughflow by 8 Sv. The deep ocean (annual and global mean at 4000 m depth) has become somewhat colder (by 0.13 C) and fresher (by 0.026) with the higher resolved sea-ice component. These features hint toward an increase in the formation rate of AABW through enhanced near-boundary convection, i.e. more dense water formation through brine release over the continental shelves and subsequent flow down the continental slope in concert with entrainment of Circumpolar Deep Water (CDW) (Gordon, 1998; Whitworth et al., 1998).

3.2. CFC versus CFF

While these dynamic features along the coastline are well captured with the higher resolution, the pattern is rather unrealistic since the coastline itself is dictated by the coarse grid. One may argue that the artificial bays are due to the Arakawa E-grid in conjunction with spherical latitude-longitude coordinates; this, however, would also be an issue with any other non-curvilinear, spherical grid. To improve this situation, especially in order to capture coastal polynyas at least as accurately as the finer grid allows for, we introduced the method described in Section 2. This constitutes the CFF version of our model. The original (coarse) coastline, the newly "excavated" (coarse) coastline, as well as the new (fine) SSM/I-based "coastline", are illustrated in Fig. 7.

The performance of CFF in terms of sea-ice variables is shown in Fig. 5. While features such as the sharp ice edge and more detail in the ice-thickness field in CFF are similar to CFC (Fig. 4), the ice-thickness distribution itself became much more realistic, at least in the Weddell Sea, e.g. when evaluating this against measurements with upward-looking sonars (Strass and Fahrbach, 1998; Harms et al., 2001). Furthermore, the pattern of the ice extent has changed, being somewhat more realistic in the Weddell Sea, and somewhat less realistic in the Ross Sea when comparing to the satellite data (Fig. 6).

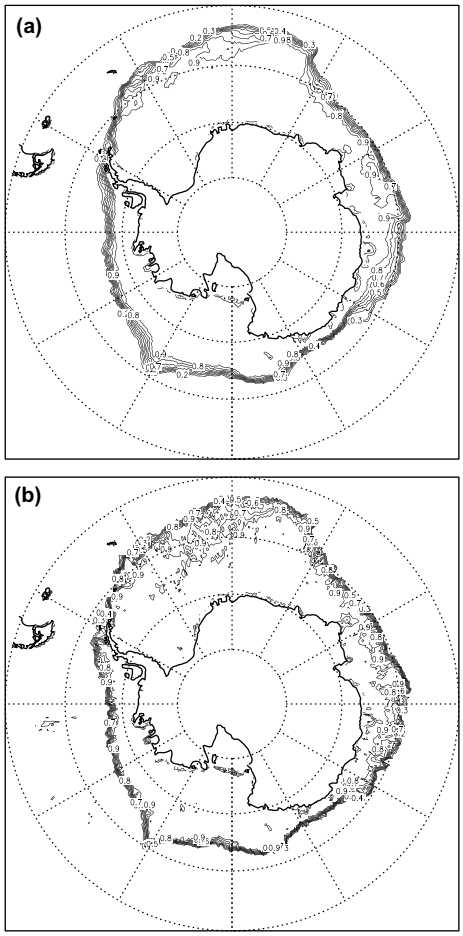

Fig. 6. Year 1992 September mean (a) and mid-September (b) ice concentration, as derived from SSM/I data using the NASA Team 2 algorithm, displayed at the highest available resolution (about 30 km).

Note that for the reason given in Section 2, the differences between CFC and CFF are not solely due to the coastal areas being better resolved. As can be extracted from Table 1, the deep ocean in CFF has become substantially cooler and fresher than in CFC, while the overall circulation in terms of the Antarctic Circumpolar Current (ACC) and the NADW outflow slowed down markedly. These features suggest a much stronger dominance of AABW in the world's ocean, and a considerably reduced density gradient across the ACC. These tendency changes associated with the switch from CFC to CFF go in the same direction as with the switch from CCC to CFC, only that they are much stronger with the former.

Further details of the ice-thickness distribution achieved with CFF can be identified in Fig. 5c versus 4c. There is a pronounced improvement in CFF over CFC in that the spurious pattern of accumulated ice in coarse grid bays has vanished. The degree of detail becomes more evident when zooming in on a coastal strip along Antarctica, e.g. in the Weddell Sea (Fig. 8), showing both ice thickness and ice velocity. Since coastal polynyas are the regions where most brine is formed, an

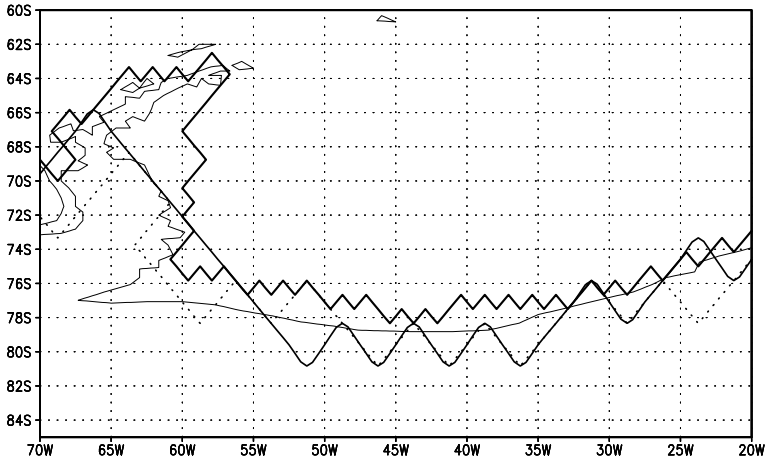

Fig. 7. Coastline representation of the original coarse grid (thin solid line), the excavated grid where it differs from the original grid (dotted line), and the SSM/I-derived grid (thick solid line).

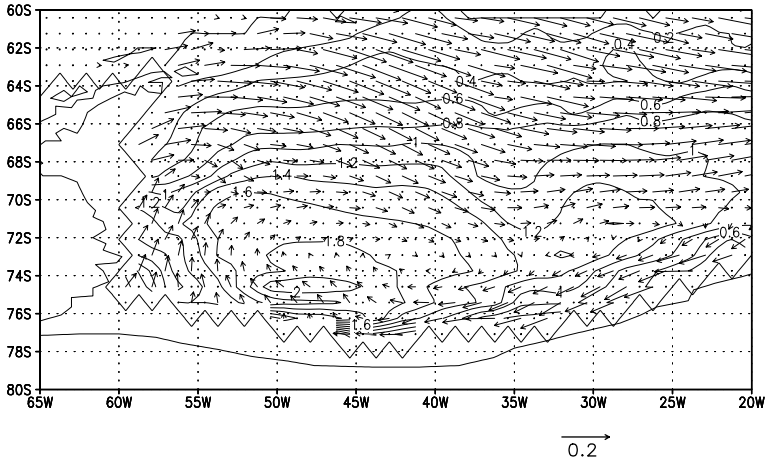

Fig. 8. September mean ice thickness and velocity in the western Weddell Sea as simulated with CFF. The ice-thickness increment is 0.2 m. The reference arrow represents 0.2 m/s.

enhanced resolution of their model representation is essential if the global properties and circulation of the deep ocean are to be captured realistically in a global model. It is also obvious that a further enhancement of the resolution is desirable.

4. Discussion

The following analysis is to explore the reasons for the differences between CFC and CCC as listed in Table 1. One expectation of enhancing the sea-ice resolution is that an overall larger lead fraction will emerge, in particular where it decisively determines the heat fluxes, namely in fall and

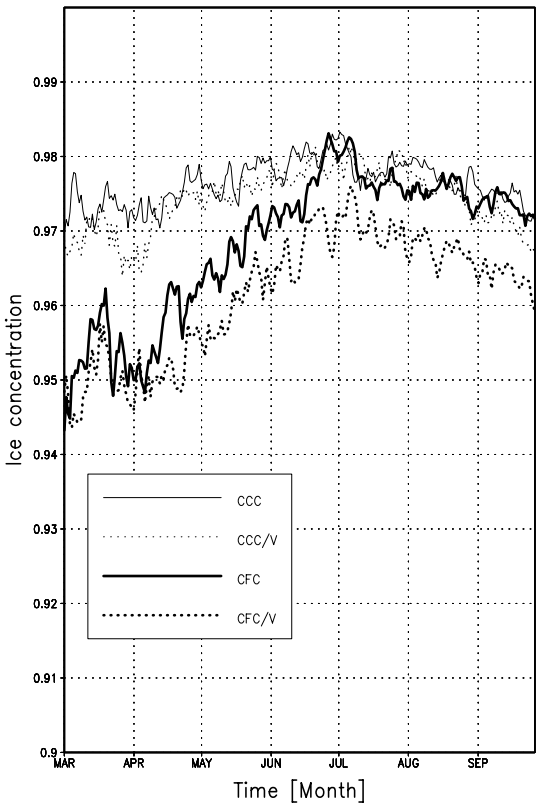

Fig. 9. March–September ice concentration south of 60 S for where and when it is in excess of 90% for simulations as indicated (see text).

winter in regions where the ice concentration is high. This is shown in Fig. 9, where the average fall and winter ice concentration in the 90–100% range south of 60 S is plotted. [2] As is obvious, the ice concentration of CFC is always smaller than that of CCC, temporarily (in particular during the ice growth season in fall) by up to 3%.

The associated change in the distribution of temperature and salinity is shown in Fig. 10 as annual and zonal averages (between 60 W and 20 E) for the Atlantic Ocean. Besides the deep-ocean cooling and freshening already seen from Table 1, the change from CFC to CCC does also involve meridional shifts in the distribution of the major water masses. The cooling and freshening between 1500 and 3500 m around 25 S reflects the weakened NADW outflow. The warming and salinification between 500 and 2000 m at around 70 S reflects a more pronounced (and more realistic) CDW signal, which is consistent with less open-ocean convection (Fig. 11), and consistent with the apparent reduction of plume convection noticed in Section 3.1. As a result of the stronger

[2] Within one model time step, the prognostic sea-ice variables are calculated in the sequence ice dynamics then thermodynamics. If lead formation due to dynamics is to be shown, it is important to extract ice concentration before thermodynamics are calculated, since a lead may easily freeze over within one model time step (which is 20 h in this model).

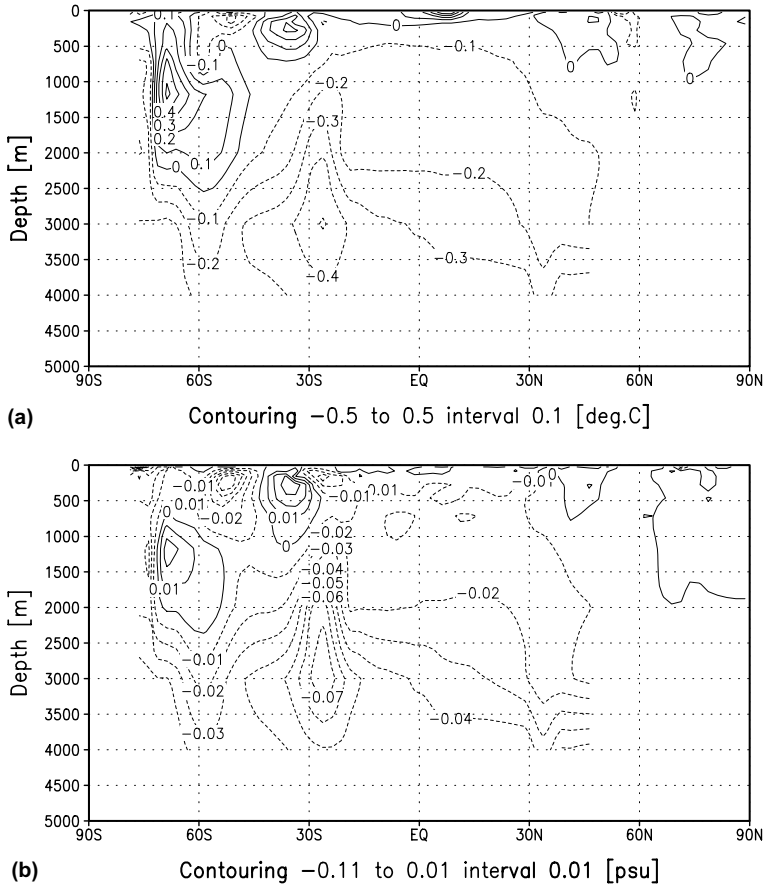

Fig. 10. Difference of Atlantic annual and zonal mean potential temperature (a) and salinity (b), CFC minus CCC.

stratification in the open-ocean part of the Weddell Sea, more freshwater is retained in the surface layers, ultimately contributing to a more pronounced (and more realistic) Antarctic Intermediate Water (AAIW) signal between the surface and 1000 m depth around 55 S. The colder and fresher water along the Antarctic continental margin reflects stronger AABW formation by near-boundary convection with less CDW entrainment. The warming south of 60 S is the main driver in reducing the meridional density gradient across the latitudes of the ACC, thus reducing its strength. The enhanced northward intrusion of AABW across 30 S leads to the reduction of the NADW outflow, a correlation that has been noticed and discussed in earlier studies (e.g., Seidov et al., 2001; Stössel and Kim, 2001; Stössel et al., 2002). When interpreting these results, it should be noticed that a large part of the changes south of 60 S are due to what is going on between 10 W and 10 E, i.e. in a geographic region that is representative of East Antarctica, where the continental shelf is very narrow and thus mostly not resolved as such in the model.

To explore the reasons for these discrepancies between CCC and CFC, additional experiments have been conducted. Since sea ice responds dynamically mainly to winds as opposed to currents (except when tidal currents are considered), one might expect larger differences due to resolution

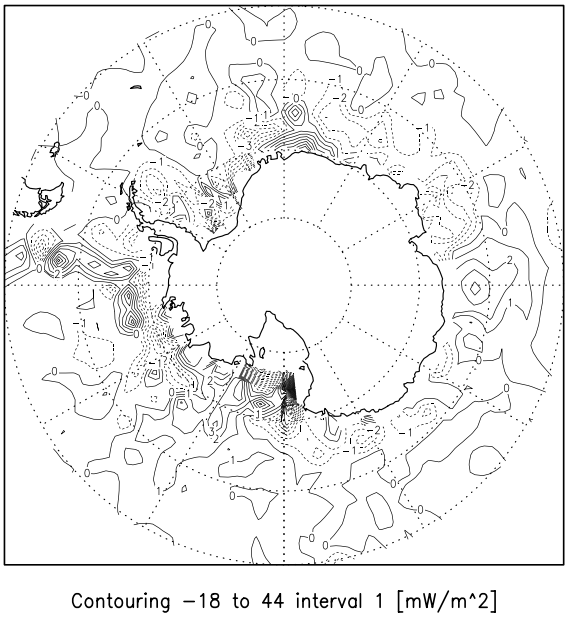

Fig. 11. Difference in annual mean convective potential energy release, CFC minus CCC.

to occur when the winds are resolved on a finer scale, or when they feature higher variability in time. Here, such has been introduced in form of an idealized pattern. In experiments CCC/V and CFC/V listed in Table 1 (where V stands for Variability), the wind variability over Southern Ocean sea ice has been enhanced by adding 0.06 N/m^2 to the wind-stress components of every other grid point in zonal direction, and by subtracting the same amount from the wind-stress components of the respective grid points in between. In addition to this spatial variability, the temporal variability of the winds has been enhanced by alternating the sign of the induced spatial anomaly pattern every time step. Note that this modification creates also additional variability in wind direction. The idea here is to induce more opportunities for the sea-ice pack to diverge and converge with the expectation that more leads would be created, as is common in nature, e.g. in conjunction with the passage of weather fronts or with tidal currents (e.g., Padman and Kottmeier, 2000). One would further expect the associated dynamic sea-ice processes of lead formation and ridging to be the better simulated the higher the resolution of the wind forcing and the sea-ice model component. The expected reduction of ice concentration, in particular where the ice is rather compact, is indicated in Fig. 9 (dashed lines).

The enhanced wind variability leads to similar tendencies in both the coarse and the fine sea-ice model versions (i.e., CCC/V versus CCC and CFC/V versus CFC) (Table 1). In CCC/V, there is a slight cooling (by 0.15 C versus CCC) of the deep ocean, but at the same time a slight increase in salinity (by 0.009). This in conjunction with a slight increase of the ACC (by 3 Sv) and a reduction of the NADW outflow (by 0.6 Sv) points toward enhanced AABW formation by open-ocean convection, as opposed to such by near-boundary convection as retrieved from the comparison of CFC with CCC. This is supported by the temperature and salinity sections showing the difference between CCC/V and CCC (Fig. 12), where the pattern of change deviates considerably from that

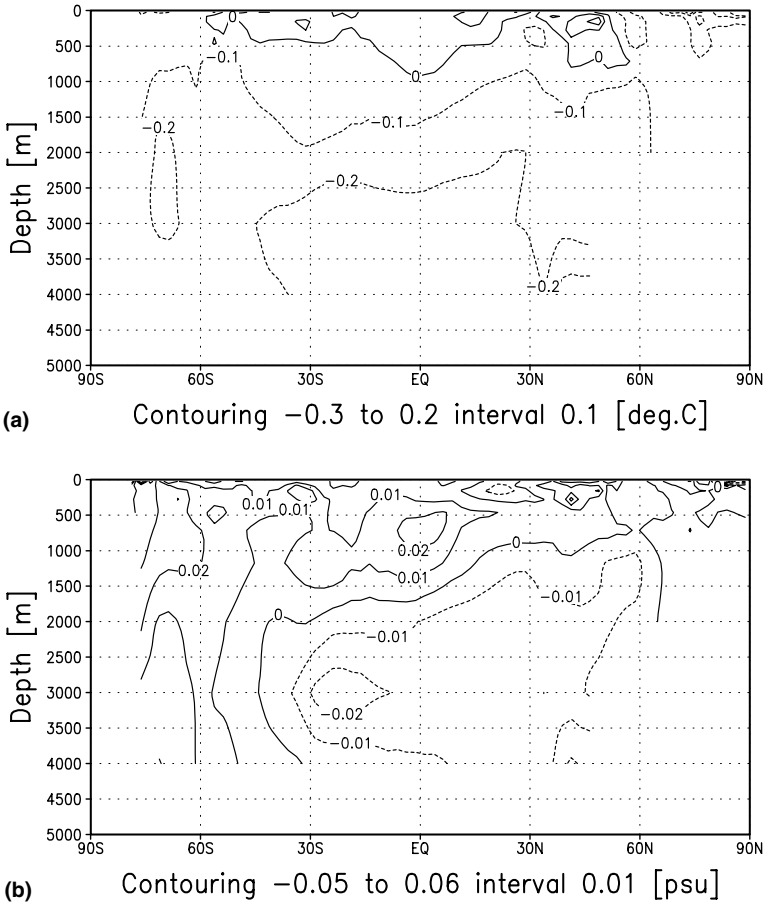

Fig. 12. Same as Fig. 10, but CCC/V minus CCC.

of Fig. 10, in particular with the Southern Ocean south of 60 S being colder in CCC/V than what resulted with CFC. That is, with CCC/V, the deep ocean becomes overall denser and the density gradient across the ACC increases due to waters south of the ACC becoming less stratified and denser because of enhanced open-ocean convection.

To identify what role an enhanced lead fraction in compact sea ice plays in changing the global deep-ocean properties, such has been introduced directly in experiments CCC/L and CCC/CP (L standing for Lead, and CP for Coastal Polynya), by reducing the ice concentration by 3% where it exceeds 90% and when/where the air temperature is below the freezing point. In CCC/L, this measure has been introduced everywhere over the Southern Ocean sea ice, while in CCC/CP, this has only been assumed for the grid points adjacent to Antarctica. The direction of change of the choke point numbers are the same as with CCC/V, while the changes themselves are stronger, in particular with CCC/L. In terms of the Atlantic meridional sections of temperature and salinity (Fig. 13), there is also a much stronger response than with CCC/V, while the pattern of change is remarkably similar to CCC/V. The pattern of CCC/CP minus CCC is similar to CCC/L minus CCC, with the numbers of change being about half of that in Fig. 13 (not shown). The pattern

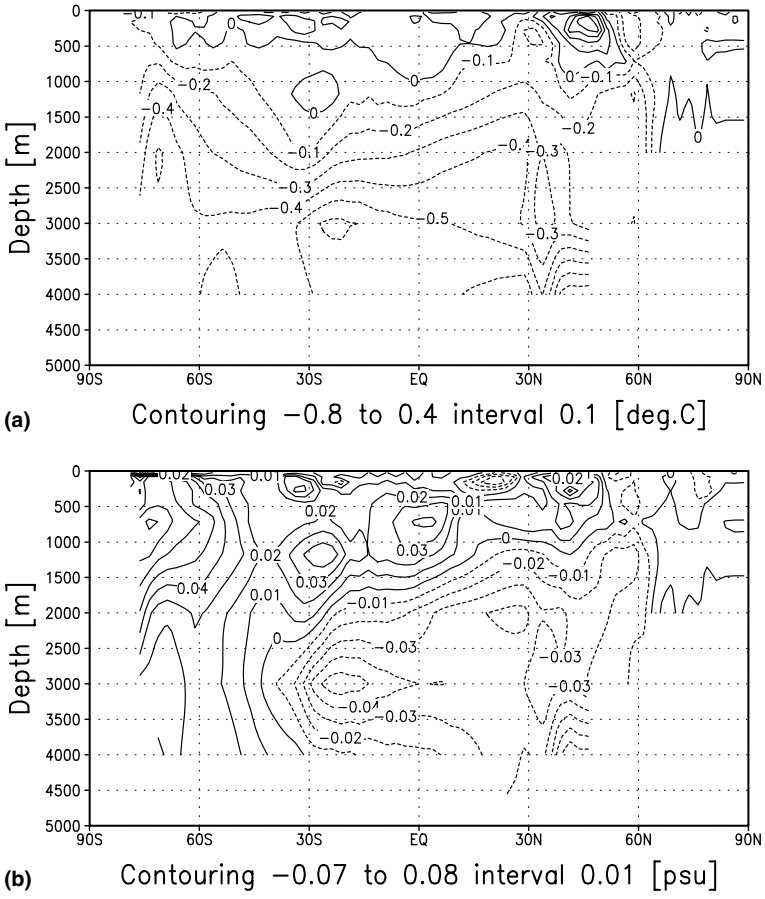

Fig. 13. Same as Fig. 10, but CCC/L minus CCC.

of cooling and salinification in the Southern Ocean is thus very different from that of CFC minus CCC (Fig. 10). The overall pattern seen in Fig. 13 indicates enhanced AABW formation by enhanced open-ocean convection (not shown). The associated enhanced intrusion of AABW to the north is clearly visible as a cooling and freshening of the deep waters north of 30 S, similar to Fig. 10, but with stronger vertical gradients. The latter seems to be associated with a weaker penetration of AAIW, turning the layers at around 1000 m depth noticeably saltier in CCC/L. In any case, the influence of AABW north of 30 S is stronger in CCC/L than it is in CFC, which is also reflected in a weaker outflow of NADW across 30 S. The ACC is clearly enhanced in both CCC/L and CCC/CP due to the enhanced density gradient across the ACC latitudes (Fig. 13) that results from the colder and saltier conditions south of 60 S.

While CCC/V, CCC/L, and CCC/CP yield a substantial cooling of the deep ocean versus CCC, and are in that respect similar to the response of CFC (versus CCC), they are all associated with an increase in global deep ocean salinity, as opposed to CFC, which yields a freshening. The pattern of meridional temperature and salinity change between CFC and the other three experiments also deviating considerably, neither enhanced wind variability nor an enhanced lead fraction seem to

be able to explain the behaviour of CFC. A remaining candidate that might explain the difference is the different way coastal winds are treated in CCC and CFC. As is common with all Arakawa grids (Arakawa, 1966) besides the "A-grid", the vector points are staggered to the scalar points (Fig. 1), and the coastal boundary of an ocean model is typically occupied by vector points. That is, wind vectors along a coastline will normally not have any dynamic impact on a neighboring scalar point. Ice thickness at such scalar point, e.g., will thus only be affected dynamically by neighboring offshore vector points, which in CCC is on the order of 200 km away from the coastline. In the case of the coastline of Antarctica, this may lead to the loss of important wind forcing data, such as offshore katabatic winds, the offshore component of which normally turns into an easterly component several tens of kilometers off the coast (Parish and Bromwich, 1991; Goodrick et al., 1998).

With the higher resolution in CFC, the coastal winds have been included to provide each fine grid point with its own wind forcing (see Section 2). Irrespective of how reliable any coastal, katabatic winds of Numerical Weather Prediction (NWP) center analyses actually are (e.g., Broeke et al., 1997; Renfrew et al., 2002), CFC contains additional wind information along the Antarctic coastline that presumably leads to a more accurate wind forcing and thus a more accurate model representation of coastal polynyas, which are critical for the process of AABW formation. We thus conducted

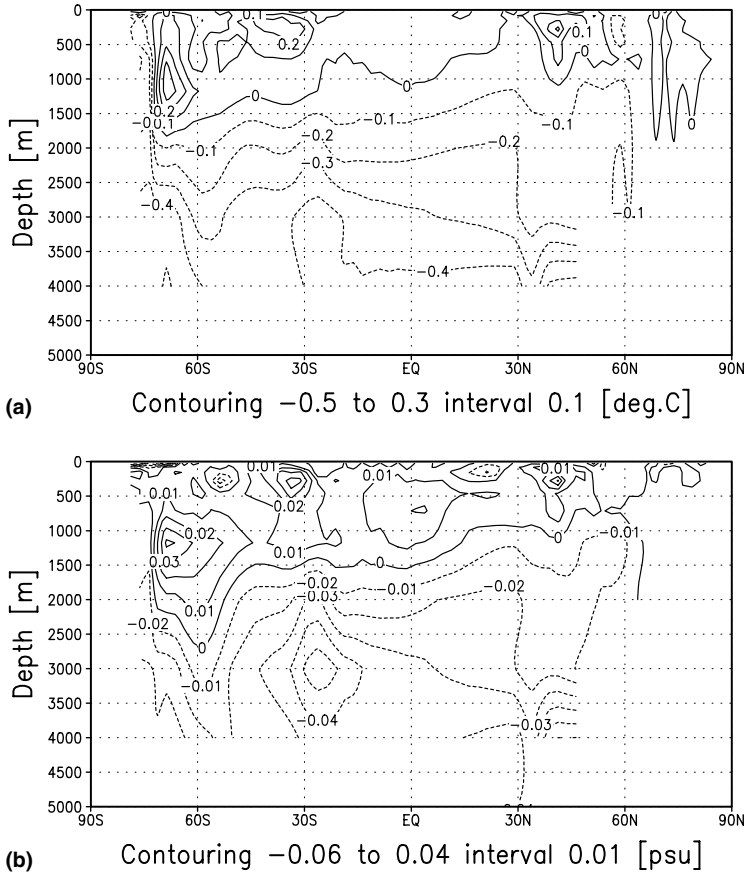

Fig. 14. Same as Fig. 10, but CCC/K minus CCC.

experiment CCC/K (where K stands for Katabatic), in which a coastal scalar point that is dynamically forced by just one (offshore) vector point, will have the wind stress on that vector point modified such that it includes the wind stress information of the adjacent three coastal vector points.

Table 1 and Fig. 14 reveal that this modification is indeed crucial for attaining the type of pattern seen in CFC versus CCC. The additional wind information, mostly reflecting offshore (katabatic) winds, works such that it enhances near-boundary convection through enhanced brine release by sea-ice formation in coastal polynays, while the newly created sea ice seems to provide the appropriate amount of meltwater in the open-ocean region (Weddell Sea) to prevent the water column from becoming excessively unstable, thus more realistically maintaining the core properties of CDW south of 60 S. The overall fresher upper layers and the more pronounced AAIW signal in CFC compared to CCC/K is consistent with open-ocean convection being more reduced in CFC versus CCC (Fig. 11) than in CCC/K versus CCC (not shown). This also leads to a noticeably reduced ACC in CFC, and a slightly enhanced ACC in CCC/K.

As noted in Section 3.2, the larger discrepancies in CFF cannot be unambiguously related to the refined coastline. The changes versus CCC (and CFC) are nevertheless characterized by the same processes that explain the difference between CFC and CCC, only that they are much stronger in CFF. The difference in convective potential energy release between CFF and CCC reveals a pattern that is similar to Fig. 11, but more pronounced (not shown), reflecting a larger reduction of open-ocean convection. The substantial cooling and freshening of the deep ocean is a result of enhanced AABW formation through enhanced near-boundary convection. In this simulation, the locations of the associated source-water mass formation sites should have the closest possible geographic correspondence to the real world under the given resolution.

5. Conclusions

This study was to demonstrate that enhancing the resolution of the sea-ice component of a global coarse-resolution ocean GCM is a viable option for improving the critical high-latitude surface buoyancy forcing while retaining the necessary efficiency of the model to investigate the long-term global deep-ocean response. The presented 9-fold resolution enhancement constitutes an intermediate step toward an 81-fold enhancement, at which point the pixel resolution of satellite passive microwave data that is routinely used to retrieve sea-ice concentration (Gloersen et al., 1992; Markus and Cavalieri, 2000) is reached. The ultimate goal is to verify the simulated sea-ice concentration on the same space and time scale as available from satellite-derived data, which is a step toward systematically identifying problems in coupled atmosphere—sea-ice—ocean GCMs.

The higher-resolution sea-ice component reveals a more detailed sea-ice texture, associated, in particular, with a more detailed representation of coastal polynyas and a sharper ice edge, both of which are in better agreement with observations. The higher resolution results also in a more realistic ice-thickness distribution in the Weddell Sea, which encompasses multi-year ice. Compression and polynya formation along the coarse coastline are physically realistic. The coastline has been adjusted to the finer grid in an additional model version, where coastal grid points have been partially covered by pseudo fast ice following the sea-ice/ocean–ice-shelf/land demarkation line of the satellite-microwave data. This measure ensures the closest possible geographical matching of coastal polynya occurrence.

The long-term global deep-ocean impact of enhancing the resolution of Southern Ocean sea ice is relatively small, but noticeable. While a major impact of this measure is an overall reduced sea-ice concentration, an according enhancement of the wind variability or an according reduction of ice concentration led to a global response pattern that is different from that associated with the higher sea-ice resolution. In particular, the pattern of the former two was more representative of one that is associated with enhanced AABW formation through enhanced open-ocean convection, as opposed to the one seen with the higher-resolution sea-ice component, which indicated less open-ocean convection, and more near-boundary convection instead. The decisive reason for this behaviour turned out to be the incorporation of the coastal winds in the higher resolution model version, which were idle in the coarse resolution version. This result demonstrates that a detailed description of the coastal (in particular katabatic) winds along Antarctica plays a vital role in determining long-term global deep-ocean properties and circulation through their direct impact on brine release due to freezing in coastal polynays and its ultimate impact on the formation of AABW. This study also showed that the formation of AAIW is getting affected by the resolution of the sea-ice component.

Major drawbacks of the current approach include the fact that the atmospheric variables are prescribed. The failure of, e.g., the winter-time air temperature to adjust to a wider polynya will severely overestimate the freezing rate therein. On the other hand, it is not even clear under what assumption on the ambient conditions such a temperature is compiled (e.g., Renfrew et al., 2002; Vihma et al., 2002). The same kind of uncertainty resides with the representation of katabatic winds in NWP analyses. There is also a large uncertainty associated with the freshwater flux as related to the precipitation rates, which modify the snow's insulation effect as well as snow-ice formation (e.g., Powell et al., 2004), and finally its direct impact on the stability of the water column (e.g., Marsland and Wolff, 2001).

Considering the general heterogeneity of a sea-ice cover, one might expect that the strength of the coupling with the atmosphere will change if the ice texture is represented on finer scales. This arises mainly due to the spatially highly inhomogeneous surface variables. E.g., the surface temperature over snow-covered ice can be -30 °C in wintertime, while at the same time it is -2 °C in a lead. This yields two totally different atmospheric boundary layers, the heat fluxes of the former being such that the surface is essentially decoupled from the atmosphere, while the latter features a highly unstable and strongly coupled situation associated with a major heat loss and thus new-ice formation in the lead. The heat and fresh-water flux forcing of the ocean will thus depend sensitively on the lead fraction (and distribution) and thus ice concentration, which is a prognostic variable of the sea-ice model. Responses to given atmospheric variables or interactions with an atmospheric GCM are thus expected to change with the resolution of a sea-ice model.

A gradual improvement of NWP center (re)analyses, a refinement of the sea-ice grid including the coastline, and an interactive description of the atmospheric forcing fields in a global ocean GCM designed for long-term integrations, will yield ever more reliable estimates on the crucial impact of southern high-latitude processes on intermediate- and deep-ocean climate.

Acknowledgements

The authors would like to acknowledge the constructive criticism of two anonymous reviewers, which widened the scope of this paper considerably. The NASA Team 2 satellite passive

microwave data were kindly provided by Thorsten Markus from Goddard Space Flight Center, and processed by Marion Stössel. This research was mainly sponsored through NASA's research grant NAG5-10641, and to some extent through NSF's research grant ATM-0333341.

References

Arakawa, A., 1966. Computational design for long-term numerical integration of the equations of fluid motion: two-dimensional incompressible flow. Part I. J. Comput. Phys. 1, 119–143.

Beckmann, A., Hellmer, H.H., Timmermann, R., 1999. A numerical model of the Weddell Sea: Large-scale circulation and water mass distribution. J. Geophys. Res. 104, 23375–23391.

Broeke, M.R., Wal, R.S.W., Wild, M., 1997. Representation of Antarctic katabatic winds in a high-resolution GCM and a note on their climate sensitivity. J. Clim. 10, 3111–3130.

Broecker, W.S., 1997. Themohaline circulation, the Achilles Heel of ourclimate system: will man-made CO2 upset the current balance? Science 278, 1582–1588.

Carmack, E.C., 1990. Large-scale physical oceanography of polar oceans. In: Polar Oceanography, Part A: Physical Science. Academic Press, pp. 171–222.

Comiso, J.C., 1995. SSM/I Sea Ice Concentrations Using the Bootstrap Algorithm, NASA Reference Publication 1380.

Comiso, J.C., Gordon, A.L., 1998. Interannual variability in summer sea ice minimum, coastal polynyas and bottom water formation in the Weddell Sea. Antarctic sea ice: physical processes, interactions and variability. AGU, Antarctic Res. Ser. 74, 293–315.

Drijfhout, S.S., Heinze, C., Latif, M., Maier-Reimer, E., 1996. Mean circulation and internal variability in an ocean primitive equation model. J. Phys. Oceanogr. 26, 559–580.

Duffy, P.B., Eby, M., Weaver, A.J., 1999. Effects of salt rejected during formation of sea ice on results of a global ocean-atmosphere-sea ice climate model. Geophys. Res. Let. 26, 1739–1742.

Eisen, O., Kottmeier, C., 2000. On the importance of leads in sea ice to the energy balance and ice formation in the Weddell Sea. J. Geophys. Res. 105 (C6), 14045–14060.

Feser, F., Weisse, R., von Storch, H., 2001. Multi-decadal atmospheric modeling for Europe yields multi-purpose data. EOS 82 (28), 305–310.

Fox, A.D., Maskell, S.J., 1996. A nested primitive equation model of the Iceland-Faeroe front. J. Geophys. Res. 101 (C8), 259–278.

Gloersen, P., Campbell, W.J., Cavalieri, D.J., Comiso, J.C., Parkinson, C.L., Zwally, H.J., 1992. Arctic and Antarctic sea ice, 1978–1987: Satellite passive microwave observations and analysis. Spec. Publ., NASA SP-511, NASA, Washington, DC.

Goodrick, S.L., McNider, R.T., Schroeder, W.W., 1998. On the interaction of the katabatic-land-sea wind system of Antarctica with the high latitude Southern Ocean. In: Jacobs, S.S., Weiss, R.F. (Eds.), Ocean, ice, and atmosphere: interactions at the Antarctic continental margin. Antarctic Res. Ser. 75, 51–65.

Goosse, H., Fichefet, T., 2001. Open-ocean convection and polynya formation in a large-scale ice-ocean, model. Tellus 53A, 94–111.

Goosse, H., Campin, J.-M., Tartinville, B., 2001. The sources of Antarctic bottom water in a global ice-ocean model. Ocean Modell. 3, 95–108.

Gordon, A.L., 1998. Western Weddell Sea thermohaline stratification. In: Jacobs, S.S., Weiss, R.F. (Eds.), Ocean, ice, and atmosphere: interactions at the Antarctic continental margin. Antarctic Res. Ser. 75, 215–240.

Griffies, S.M., Boening, C., Bryan, F.O., Chassignet, E.P., Gerdes, R., Hasumi, H., Hirst, A., Treguier, A.-M., Webb, D., 2000. Developments in ocean climate modelling. Ocean Modell. 2, 123–192.

Harms, S., Fahrbach, E., Strass, V.H., 2001. Sea ice transports in the Weddell Sea. J. Geophys. Res. 106, 9057–9073.

Hibler, W.D., 1979. A dynamic thermodynamic sea ice model. J. Phys. Oceanogr. 9, 815–846.

Jacob, D., Podzun, R., 1997. Sensitivity studies with the regional climate model REMO. Meteorol. Atmos. Phys. 63, 119–129.

Kalliosaari, S., Seinä, A., 1987. Ice winters 1981–1985 along the Finnish coast. Finnish Marine Research No. 254, pp. 5–63.
Kim, S.-J., Stössel, A., 2001. Impact of subgrid-scale convection on global thermohaline properties and circulation. J. Phys. Oceanogr. 31, 656–674.
Maier-Reimer, E., 1993. The driving force of brine rejection on the deepwater formation in the Hamburg LSG OGCM. NATO-ASI series, Itl2, pp. 211–216.
Maier-Reimer, E., 1997. Design of a closed-boundary regional model of the Arctic Ocean. Bull. Amer. Meteor. Soc., Workshop on polar processes in global climate, 13–15 November 1996, pp. 72–73.
Maier-Reimer, E., Mikolajewicz, U., Hasselmann, K., 1993. Mean circulation of the Hamburg LSG OGCM and its sensitivity to the thermohaline surface forcing. J. Phys. Oceanogr. 23 (4), 731–757.
Markus, T., Kottmeier, C., Fahrbach, E., 1998. Ice formation in coastal polynyas in the Weddell Sea and their impact on oceanic salinity. Antarctic sea ice: physical processes, interactions and variability. AGU, Antarctic Res. Ser. 74, 273–292.
Markus, T., Cavalieri, 2000. An enhancement of the NASA Team sea ice algorithm. IEEE Trans. Geosc. and Remote Sens. 38 (3), 1387–1398.
Marshall, J., Schott, F., 1999. Open-ocean convection: observations, theory, and models. Rev. Geophys. 37, 1–64.
Marsland, S., Wolff, J.-O., 2001. On the sensitivity of Southern Ocean sea ice to the surface fresh-water flux: A model study. J. Geophys. Res. 106 (C2), 2723–2741.
Marsland, S.J., Haak, H., Jungclaus, J.H., Latif, M., Roeske, F., 2003. The Max-Planck-Institute global ocean / sea ice model with orthogonal curvilinear coordinates. Ocean Modell. 5 (2).
Mikolajewicz, U., Jungclaus, J., Haak, H., 2001. Simulating the ocean response to atmospheric variability. WMO/TD-No. 1064, Report No. 31, pp. 9.18–9.19.
Orsi, A.H., Jacobs, S.S., Gordon, A.L., Visbeck, M., 2001. Cooling and ventilating the abyssal ocean. Geophys. Res. Lett. 28 (15), 2923–2926.
Owens, W.B., Lemke, P., 1990. Sensitivity studies with a sea ice—mixed layer—pycnocline model in the Weddell Sea. J. Geophys. Res. 95, 9527–9538.
Padman, L., Kottmeier, C., 2000. High frequency ice motion and divergence in the Weddell Sea. J. Geophys. Res. 105, 3379–3400.
Paluszkiewicz, T., Romea, R.D., 1997. A one-dimensional plume model for the parameterisation of oceanic deep convection. Dyn. Ocean Atmos. 26, 95–130.
Parish, T.R., Bromwich, D.H., 1991. Continental-scale simulation of the Antarctic katabatic wind regime. J. Clim. 4, 135–146.
Powell, D.C., Markus, T., Stössel, A., 2004. The effects of snow depth forcing on Southern Ocean sea ice simulations. J. Geophys. Res., re-submitted.
Renfrew, I.A., King, J.C., Markus, T., 2002. Coastal polynyas in the southern Weddell Sea: variability of the surface energy budget. J. Geophys. Res. 107 (C6).
Seidov, D., Barron, E., Haupt, B.J., 2001. Meltwater and the global ocean conveyor: northern versus southern connections. Global Planetary Change 30, 257–270.
Spall, M.A., Holland, W.R., 1991. A nested primitive equation model for oceanic applications. J. Phys. Oceanogr. 21, 205–220.
Stössel, A., Kim, S.-J., 2001. Decadal deep-water variability in the subtropical Atlantic and convection in the Weddell Sea. J. Geophys. Res. 106 (C10), 22425–22440.
Stössel, A., Yang, K., Kim, S.-J., 2002. On the role of sea ice and convection in a global ocean model. J. Phys. Oceanogr. 32, 1194–1208.
Stössel, A., Markus, T., 2004. Using satellite-derived ice concentration to represent Antarctic coastal polynyas in ocean climate models. J. Geophys. Res. 109 (C02014).
Strass, V.H., Fahrbach, E., 1998. Temporal and regional variation of sea ice draft and coverage in the Weddell Sea obtained from upward looking sonars. Antarctic sea ice: physical processes, interactions and variability. AGU, Antarctic Res. Ser. 74, 123–139.
Timmermann, R., Hellmer, H.H., Beckmann, A., 2002. Simulations of ice-ocean dynamics in the Weddell Sea 2. Interannual variability 1985–1993. J. Geophys. Res., l07.

Vihma, T., Uotila, B., Cheng, B., Launiainen, J., 2002. Surface heat budget over the Weddell Sea: buoy results and model comparisons. J. Geophys. Res. 107 (C2), 2000JC000372.

Whitworth, T., Orsi, A.H., Kim, S.-J., Nowlin, W.D., Locarnini, R.A., 1998. Water masses and mixing near the Antarctic slope front. In: Jacobs, S.S., Weiss, R.F. (Eds.), Ocean, ice, and atmosphere: interactions at the Antarctic continental margin. Antarctic Res. Ser. 75, 1–27.

Wolff, J.-O., Maier-Reimer, E., Legutke, S., 1997. The Hamburg Ocean Primitive Equation model HOPE. Technical Report No. 13, Hamburg/Germany: Deutsches Klimarechenzentrum.